Electronic Supplementary Material (ESI) for ChemComm.
This journal is © The Royal Society of Chemistry 2024

Supporting Information

Iron Homo- and Heterobimetallic Complexes Supported by a Symmetrical Dinucleating Ligand

Pablo Ríos,‡[a,b] Matthew S. See,‡[b,c] Oscar Gonzalez,[b] Rex C.Handford,[b] Amélie Nicolay,[b,c] Guodong Rao,[d] R. David Britt,*[d] D. Kwabena Bediako*[b] and T. Don Tilley*[b,c]

[a]Instituto de Investigaciones Químicas (IIQ), Departamento de Química Inorgánica, Centro de Innovación en Química Avanzada (ORFEO-CINQA), CSIC and Universidad de Sevilla. Sevilla, 41092, Spain

[b]Department of Chemistry, University of California, Berkeley, USA.

[c]Chemical Sciences Division, Lawrence Berkeley National Laboratory, Berkeley, CA 94720, USA.

[d] Department of Chemistry, University of California, Davis, Davis, California 95616, United States

*Corresponding author: tdtilley@berkeley.edu

1. General considerations

Unless stated otherwise, all reactions were performed in a glovebox or on a Schlenk line under an atmosphere of pure N_2 using standard Schlenk techniques. Pentane, diethyl ether, tetrahydrofuran and acetonitrile were dried and deaerated using a JC Meyers Phoenix solvent purification system. Hexamethyldisiloxane (HMDSO) was dried over potassium before being distilled. Ethanol was dried over 3 Å molecular sieves and degassed with three freeze-pump-thaw cycles. All solvents were stored over 3 Å molecular sieves for at least 24 h prior to use. Compounds **1**,[1] **2**,[2] **3**,[2] mesityl azide[3] and $Fe(NTf_2)_2$[4] were prepared according to literature procedures. All other reagents were purchased from commercial suppliers and used as received.

NMR spectroscopy. NMR spectra were recorded on Bruker Avance 400 and 500 MHz spectrometers and are referenced to residual protio solvent for ^1H or $^{13}C\{^1H\}$ NMR spectroscopy. NMR spectra were taken at 25°C unless otherwise noted. Structural assignments were performed using HSQC and HMBC NMR spectroscopic experiments when necessary. All NMR spectra were analyzed with MestReNova.

Mass Spectrometry. Samples for ESI-MS spectrometry were prepared in MeCN in a nitrogen-filled glovebox. All ESI-MS spectra were obtained on a PerkinElmer AxION 2 UHPLC-TOF system equipped with an ESI source in the positive ionization mode.

Elemental analyses were performed by Dr. Elena Kreimer at the Microanalytical Facility in the College of Chemistry at the University of California, Berkeley, using a Perkin Elmer 2400 Series II combustion analyzer equipped for determination of %C, %H, and %N.

IR spectroscopy. Infrared spectra were recorded via ATR employing an A225/Q Platinum ATR accessory with a Bruker Vertex 80 FTIR Spectrometer equipped with a room temperature DLaTGS detector using OPUS software (v. 7.2).

DC magnetization measurements were carried out on a Quantum Design Physical Property Measurement System Dynacool equipped with a 12 T magnet using the Vibrating Sample Magnetometer option. Powders were transferred to powder sample holders which were affixed to a brass sample holder.

EPR spectroscopy. X-band (9.4 GHz) CW EPR spectra were recorded on a Bruker (Billerica, MA) EleXsys E500 spectrometer equipped with a super high Q resonator (ER4122SHQE). Cryogenic temperatures were achieved and controlled using an ESR900 liquid helium cryostat in conjunction with a temperature controller (Oxford Instruments ITC503) and gas flow controller. The CW EPR spectrum was recorded at 10 K using 0.2 mW microwave power. EPR samples of **6** were prepared at 2.0 mM in ethanol. The resulting solutions were glassed and stored in liquid nitrogen. Spectral simulation was performed in Matlab 2022b with EasySpin 6.0.0-dev package.[5]

2. Synthesis and characterization

- **2,7-bis(1-mesityl-1*H*-1,2,3-triazol-4-yl)-1,8-naphthyridine (MTN ligand)**

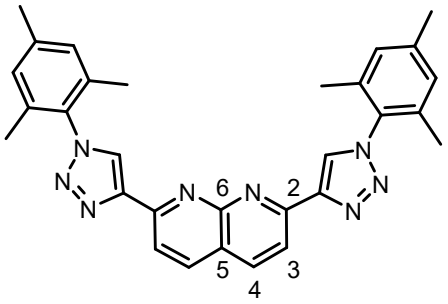

A 100 mL round-bottom flask was charged under air with a stir bar, compound **3** (230 mg, 1.29 mmol), mesityl azide (437 mg, 2.71 mmol) and ethanol (15 mL). A suspension of copper(II) sulfate (21 mg, 0.129 mmol) and L-sodium ascorbate (204 mg, 1.03 mmol) in deionized water (12 mL) was added to this mixture. A condenser was connected to the round-bottom flask, and the mixture was stirred at 60 °C for 20 hours, after which TLC analysis (CH_2Cl_2:acetone 9:1) confirmed the absence of starting material. The mixture was diluted with deionized water (20 mL) and extracted with dichloromethane (5 x 30 mL). The combined organic phases were dried over sodium sulfate, filtered, and concentrated under vacuum to give a dark orange oily solid. This residue was dissolved in the minimum volume of dichloromethane and loaded on a silica column (ø = 5-6 cm, height of silica = 12 cm). It was eluted with dichloromethane until complete separation of excess mesityl azide was confirmed by TLC analysis, then the product was eluted with dichloromethane:acetone 9:1. Volatiles were removed under vacuum, giving an orange oil that was further dried in the Schlenk line to afford pure **MTN** (600 mg, 1.20 mmol, 93% yield) as a pale yellow solid. Yellow crystals suitable for X-ray diffraction analysis can be grown by vapor diffusion of diethyl ether into a dichloromethane solution of **MTN** at 23 °C.

^{1}H-NMR (500 MHz, CD_2Cl_2, 298 K): δ 8.69 (s, 2H, triazole C–*H*), 8.51 (d, $^3J_{H\text{-}H}$ = 5.8 Hz, 2H, 4-naph C–*H*), 8.33 (d, $^3J_{H\text{-}H}$ = 5.8 Hz, 2H, 3-naph C–*H*), 6.95 (s, 4H, Mes C–*H*), 2.34 (s, 6H, Mes *p*-CH_3), 1.94 (s, 12 H, Mes *o*-CH_3) ppm. **^{13}C{^{1}H}-NMR (125 MHz, CD_2Cl_2, 298 K): δ** 156.2 (C6), 154.4 (C2), 148.3 (imidazole C_q), 140.6 (Mes C_{para}), 138.3 (C3), 135.2 (Mes C_{ipso}), 133.6 (Mes C_{para}), 129.4 (Mes C_{meta}), 126.3 (imidazole *C*-H), 122.4 (C5), 119.6 (C4), 21.3 (Mes *p*-*C*H_3), 17.4 (Mes *o*-*C*H_3) ppm.

Anal. Calcd for: $C_{30}H_{28}N_8 \cdot 0.2CH_2Cl_2$: C, 70.08; H, 5.53; N, 21.65. Found: C, 69.89; H, 5.74; N, 21.53.

- **[(MTN)$_2$Fe$_2$(μ-Cl)(THF)$_2$][NTf$_2$]$_3$ (Complex 4)**

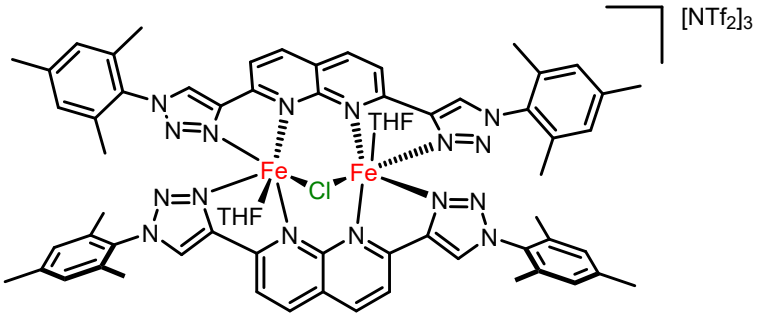

In a N_2-filled glovebox, a solution of **MTN** (100 mg, 0.200 mmol) in THF (6 mL) was added dropwise for 10 min to a 20 mL scintillation vial containing a stirring mixture of $FeCl_2$ (12.6 mg, 0.100 mmol) and $Fe(NTf_2)_2$ (92.4 mg, 0.150 mmol) in THF (4 mL). The resulting orange-red mixture was left stirring at 23 °C for 2 h, after which it was filtered (glass microfiber in a Pasteur pipette) to a 20 mL scintillation vial. The filtrate was concentrated under vacuum to approximately 5-6 mL, and it was layered with pentane (12-13 mL). The resulting bilayer was left to stand at 23 °C for 3 days, after which orange crystals suitable for X-ray diffraction analysis were observed. The supernatant was discarded, and pentane (20 mL) was added. The mixture was vigorously stirred for 1-2 hours until the crystals became an orange powder. The supernatant was carefully removed, and the orange powder was dried under vacuum to yield 182 mg of complex **4** (85% yield).

Anal. Calcd for: $C_{70}H_{64}ClF_{18}Fe_2N_{19}O_{13}S_6$ (1 THF molecule bound to Fe): C, 40.80; H, 3.13; N, 12.91. Found: C, 40.88; H, 3.25; N, 12.52.

Effective magnetic moment (PPMS, 298 K), μ_{eff} = 6.6 μ_B

- **MTN·FeCl$_2$ (Complex 5)**

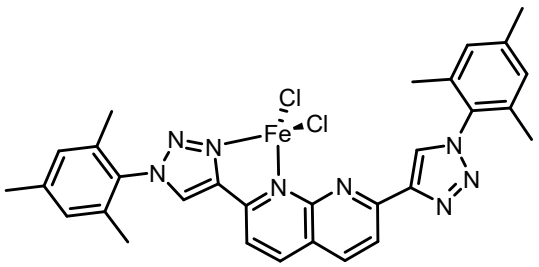

In a N_2-filled glovebox, a solution of **MTN** (80 mg, 0.160 mmol) in THF (4 mL) was added to a 20 mL scintillation vial containing $FeCl_2$ (19.3 mg, 0.150 mmol). The resulting mixture was stirred at 23 °C for 22 h, after which it became a pink suspension, which was filtered through a 15 mL fine porosity frit. The resulting pink solid collected on the frit was washed with THF (3 x 2 mL). Then, it was suspended in THF (3 mL) and transferred to a 20 mL scintillation vial, where it was dried under vacuum, giving analytically pure complex **5** as a pink powder (91.3 mg, 0.146 mmol, 97% yield).

Anal. Calcd for: $C_{30}H_{28}Cl_2FeN_8$: C, 57.44; H, 4.50; N, 17.86. Found: C, 57.32; H, 4.38; N, 17.81.
Effective magnetic moment (Evans' method, DMSO, 500 MHz), μ_{eff} = 4.9 μ_B

- **[(MTN)$_3$Fe(μ-Cl)$_2$Mn][OTf$_2$]$_2$ (Complex 6)**

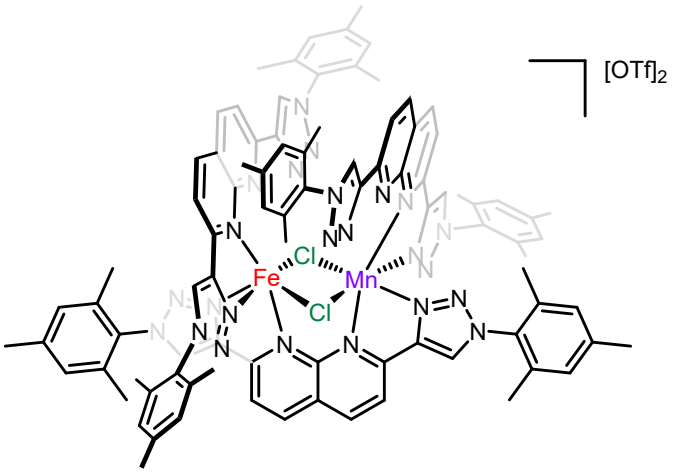

In a N_2-filled glovebox, a solution of **MTN** (24 mg, 0.0480 mmol) in THF (0.5 mL) was added to a 4 mL dram vial containing **5** (15 mg, 0.0240 mmol). MeCN (2 mL) was added, and the resulting suspension was added dropwise for 5 min to a scintillation vial containing a stirring solution of Mn(OTf)$_2$·3MeCN (10.4 mg, 0.0240 mmol) in MeCN (1 mL). The resulting orange solution was left stirring at 23 °C for 2 hours, after which it was filtered (fiber glass in a Pasteur pipette) to a 20 mL scintillation vial. The filtrate was layered with diethyl ether (13-14 mL). The bilayer was left to stand at 23 °C for 2 days, after which orange crystals suitable for X-ray diffraction analysis were observed. The supernatant was discarded, and diethyl ether (20 mL) was added. The mixture was vigorously stirred for 30 min until the crystals became a pale pink-orange powder. The supernatant was carefully removed, and the powder was dried under vacuum to yield 38 mg of complex **6** (81% yield).

Anal. Calcd for: $C_{92}H_{84}Cl_2F_6FeMnN_{24}O_6S_2$: C, 55.76; H, 4.27; N, 16.96. Found: C, 55.69; H, 4.01; N, 16.70.

Effective magnetic moment (PPMS, 298 K), μ_{eff} = 6.8 μ_B

- **[(MTN)$_3$Fe$_2$(μ-Cl)$_2$][OTf$_2$]$_2$ (Complex 7)**

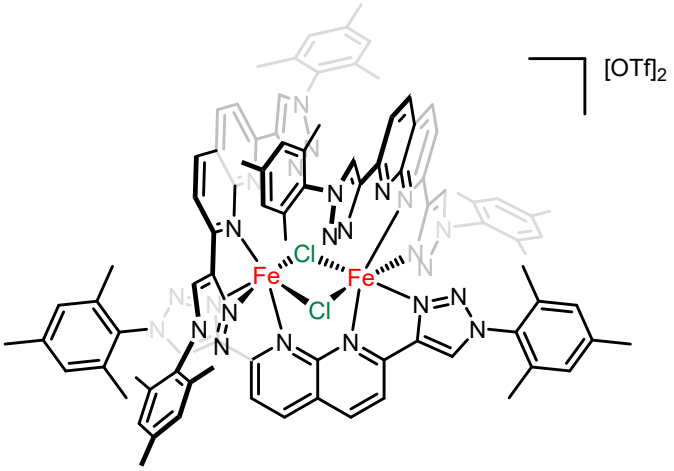

In a N_2-filled glovebox, a suspension of **MTN** (30 mg, 0.0600 mmol) in MeCN (1 mL) was added dropwise to a 20 mL scintillation vial containing a stirring mixture of $FeCl_2$ (2.5 mg, 0.0200 mmol) and $Fe(OTf)_2$ (7.1 mg, 0.0200 mmol) in MeCN (1 mL). The vial containing the ligand was rinsed with MeCN (1 mL) and the rinses were added dropwise to the reaction mixture, which was left stirring for 48 h at 23 °C. The resulting orange-red suspension was filtered through celite (1 cm height in a Pasteur pipette) to a 20 mL scintillation vial. The reaction vial and filter were rinsed with MeCN (1 mL), and the resulting red-orange filtrate was layered with diethyl ether (13-14 mL). The bilayer was left to stand at 23 °C for 2 days, after which red-orange crystals suitable for X-ray diffraction analysis were observed. The supernatant was discarded, and diethyl ether (20 mL) was added. The mixture was vigorously stirred for 30 min until the crystals became a dark pink powder. The supernatant was carefully removed, and the dark pink powder was dried under vacuum to yield 26 mg of complex **7** (66% yield).

Anal. Calcd for: $C_{92}H_{84}Cl_2F_6Fe_2N_{24}O_6S_2$: C, 55.74; H, 4.27; N, 16.96. Found: C, 55.59; H, 4.27; N, 16.77.

Effective magnetic moment (PPMS, 298 K), μ_{eff} = 6.4 μ_B

3. NMR spectra

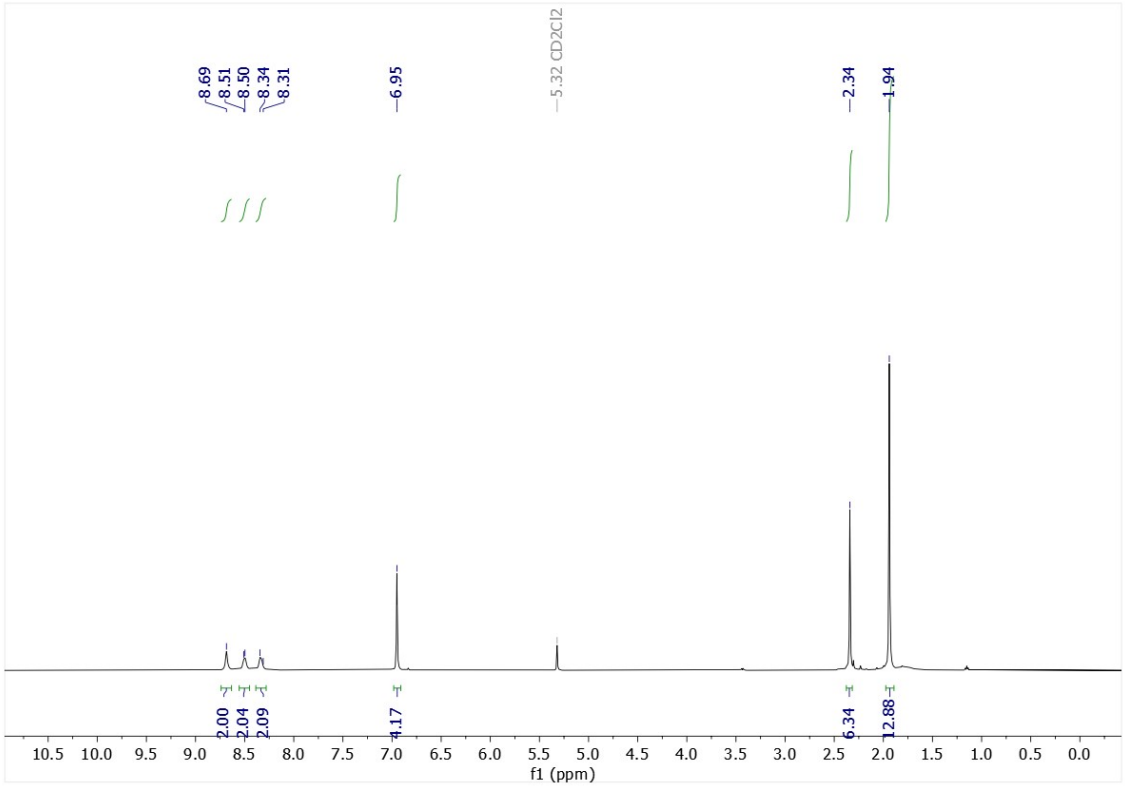

Figure S1. ^{1}H NMR spectrum (CD_2Cl_2, 500 MHz) of **MTN**.

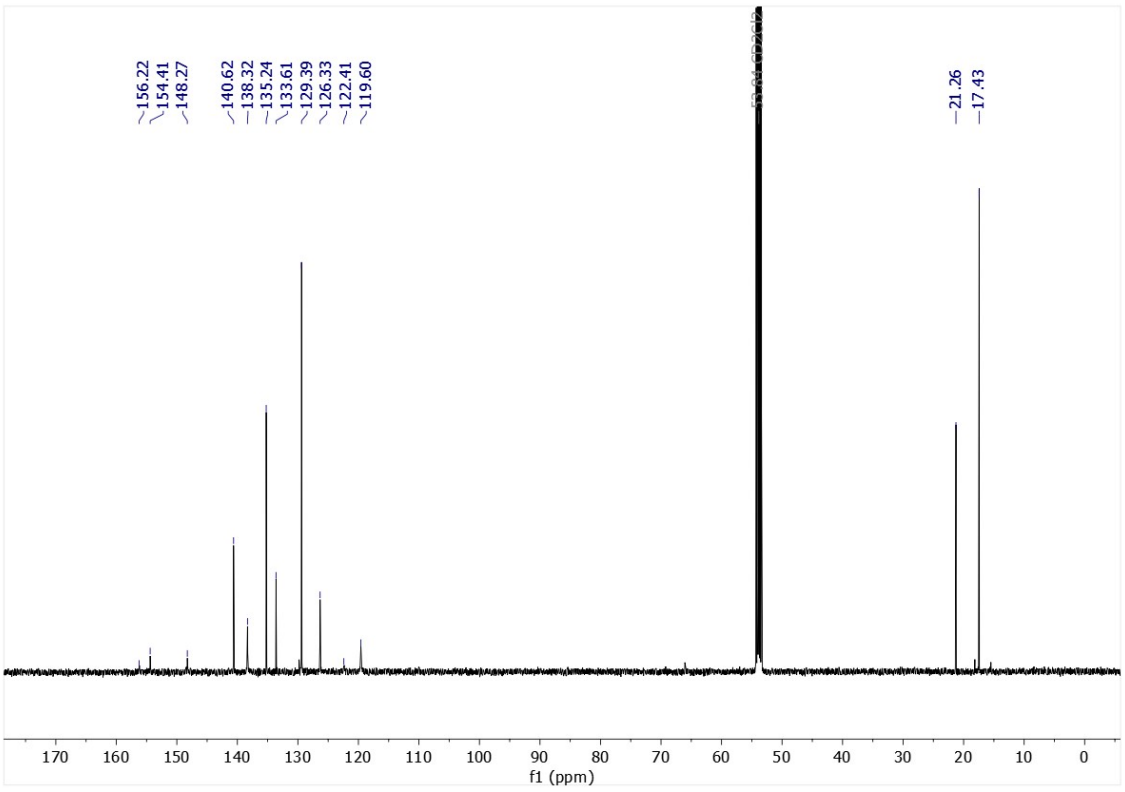

Figure S2. $^{13}C\{^{1}H\}$ NMR spectrum (CD_2Cl_2, 125 MHz) of **MTN**.

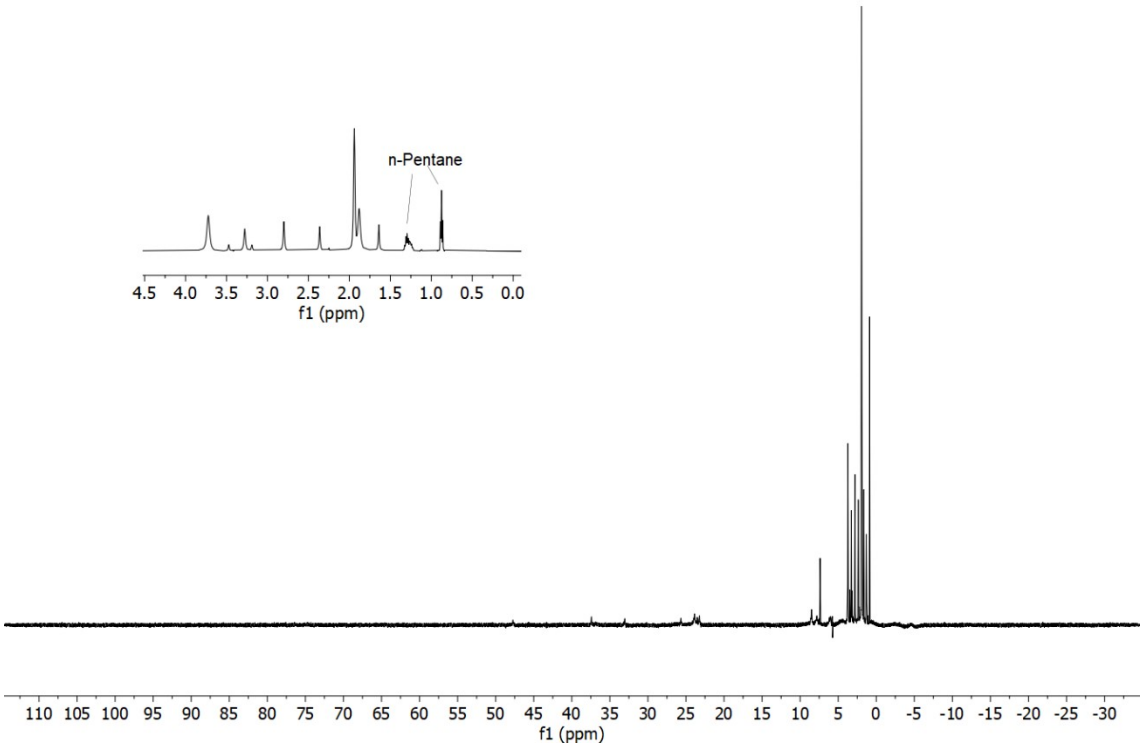

Figure S3. ^{1}H NMR spectrum (CD_3CN, 500 MHz) of **4**.

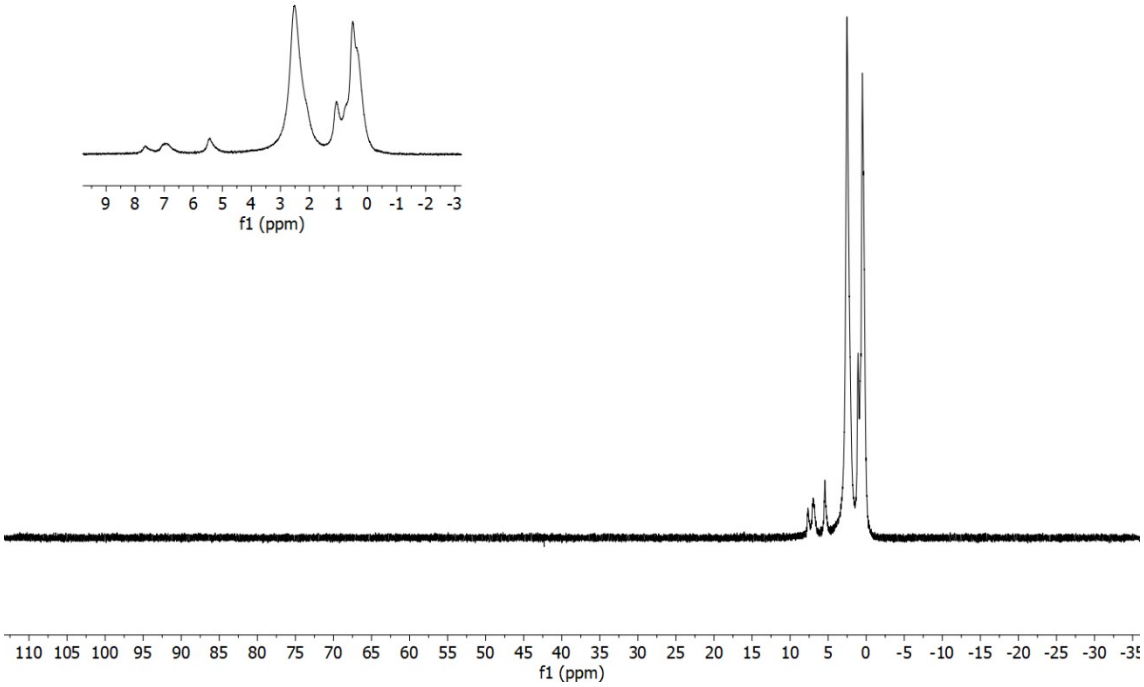

Figure S4. ^{1}H NMR spectrum (d_6-DMSO, 500 MHz) of **5**.

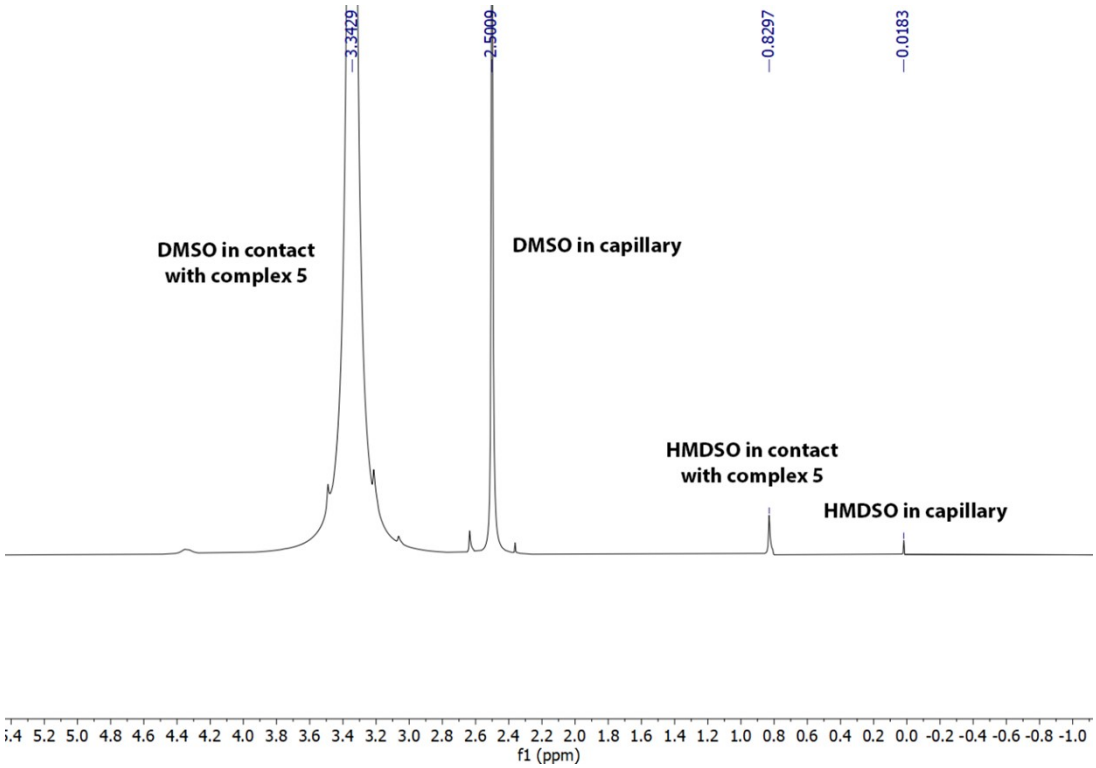

Figure S5. Effective magnetic moment determination: ^{1}H NMR spectrum (d_6-DMSO, 500 MHz, 20 °C) of **5**. A 0.05 M HMDSO (hexamethyldisiloxane) solution in DMSO was utilized as standard in a capillary, and to dissolve complex **5**. An average value (413.35 Hz) of the shifts of the DMSO (0.842 ppm, 421 Hz) and HMDSO (0.811 ppm, 405.7 Hz) resonances was considered for the determination of $\mu_{eff.}$

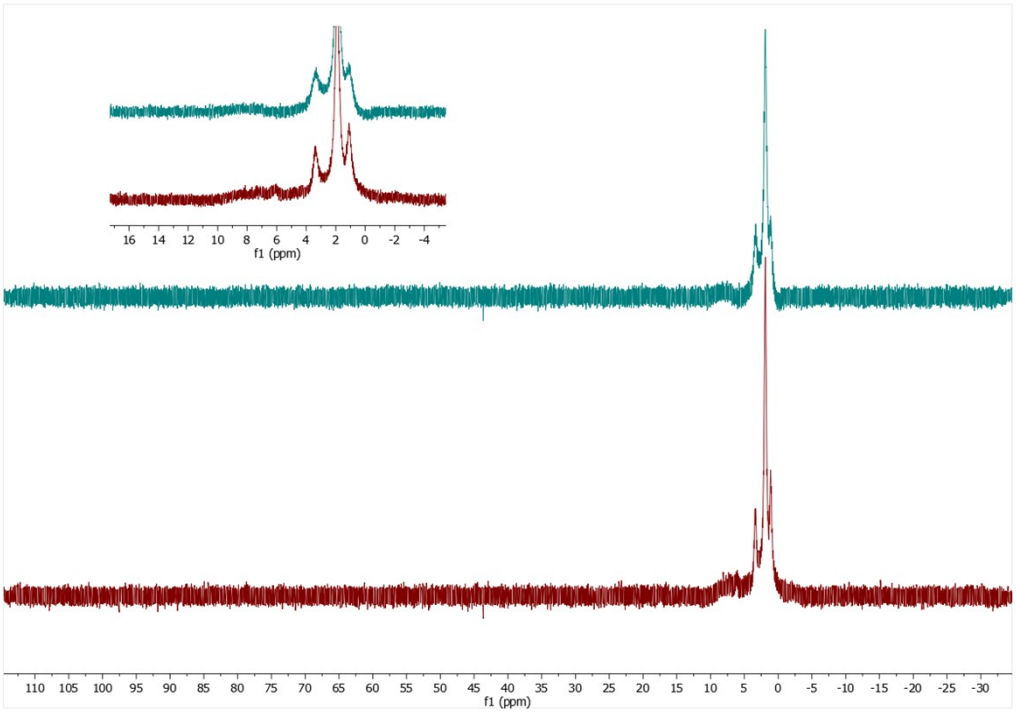

Figure S6. ^{1}H NMR spectra (CD_3CN, 500 MHz) of complexes **6** (top) and **7** (bottom).

In order to show demonstrate there is no scrambling, the NMR samples of **6** and **7** were stored in solution at 23 °C for 48 h, after which mass spectrometry analysis was performed. Similar spectra to those observed for crystalline samples (Figures S13-S16) were observed.

4. IR spectra

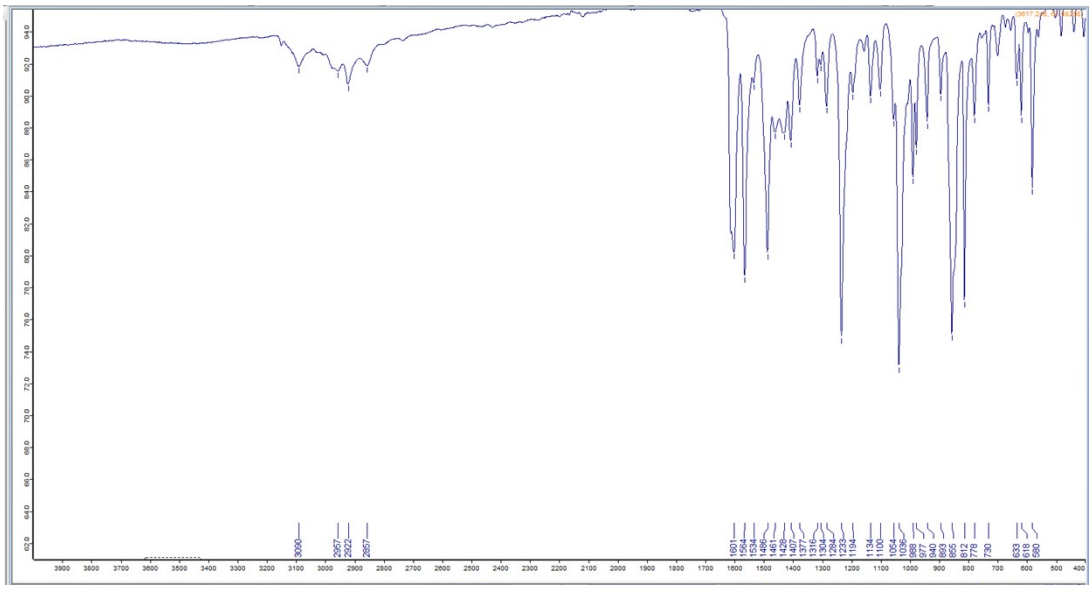

Figure S7. IR spectrum of **MTN**.

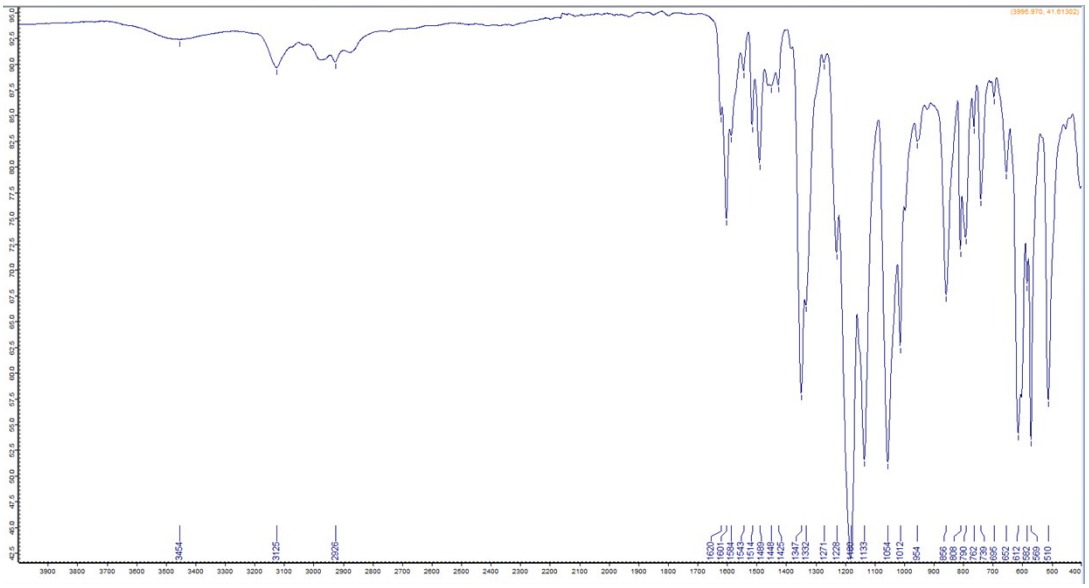

Figure S8. IR spectrum of complex **4**.

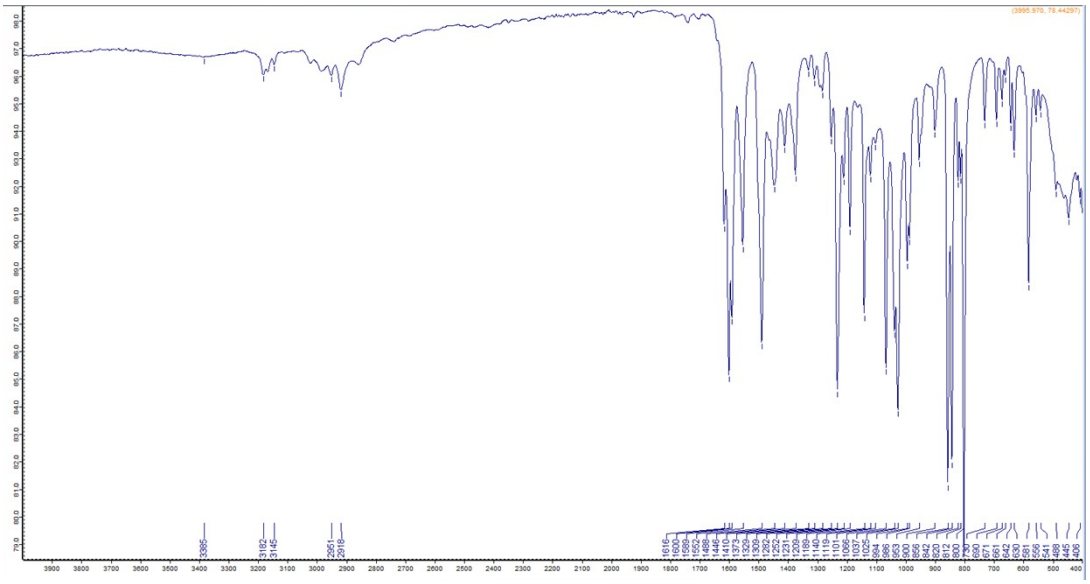

Figure S9. IR spectrum of complex **5**.

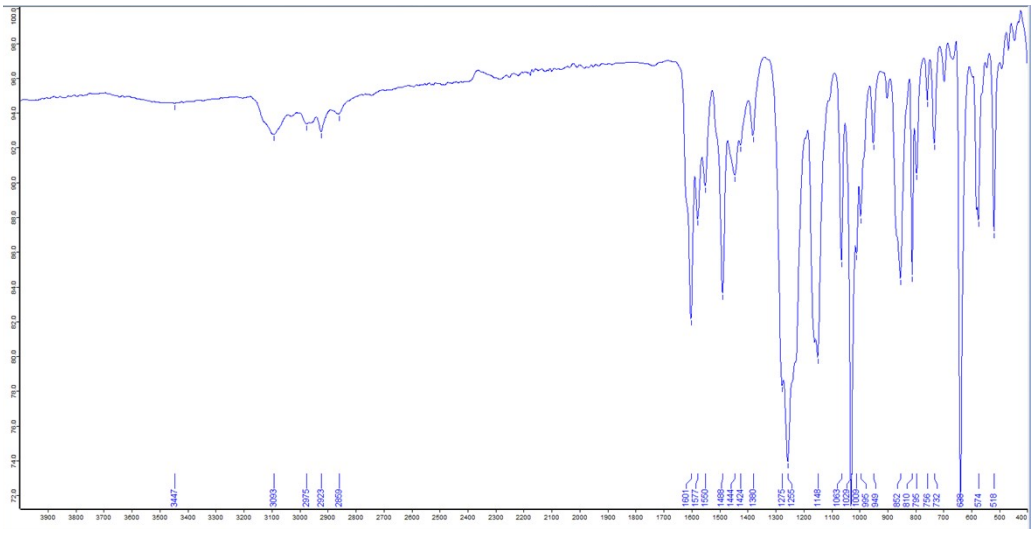

Figure S10. IR spectrum of complex **6**.

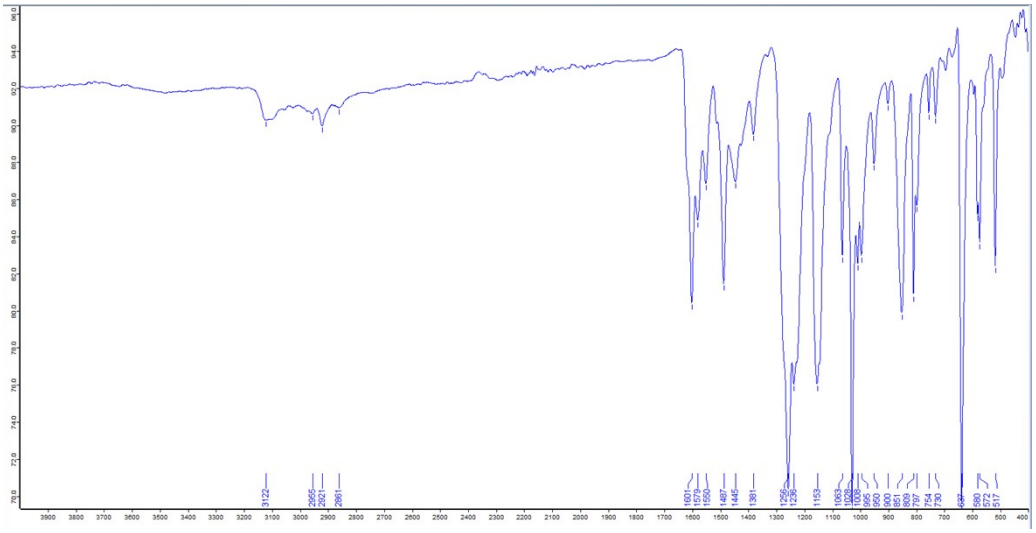

Figure S11. IR spectrum of complex **7**.

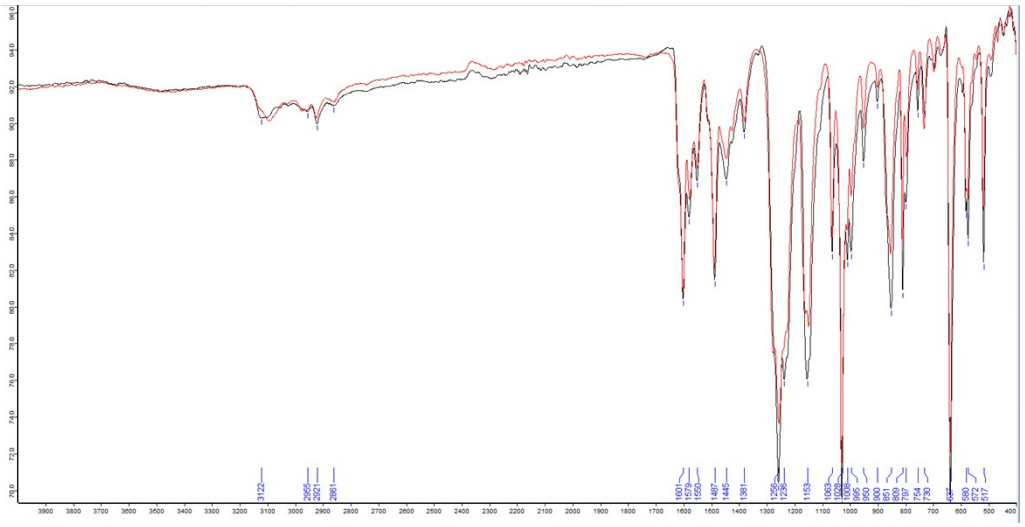

Figure S12. IR spectra of complexes **6** and **7** overlapped.

5. Mass spectra

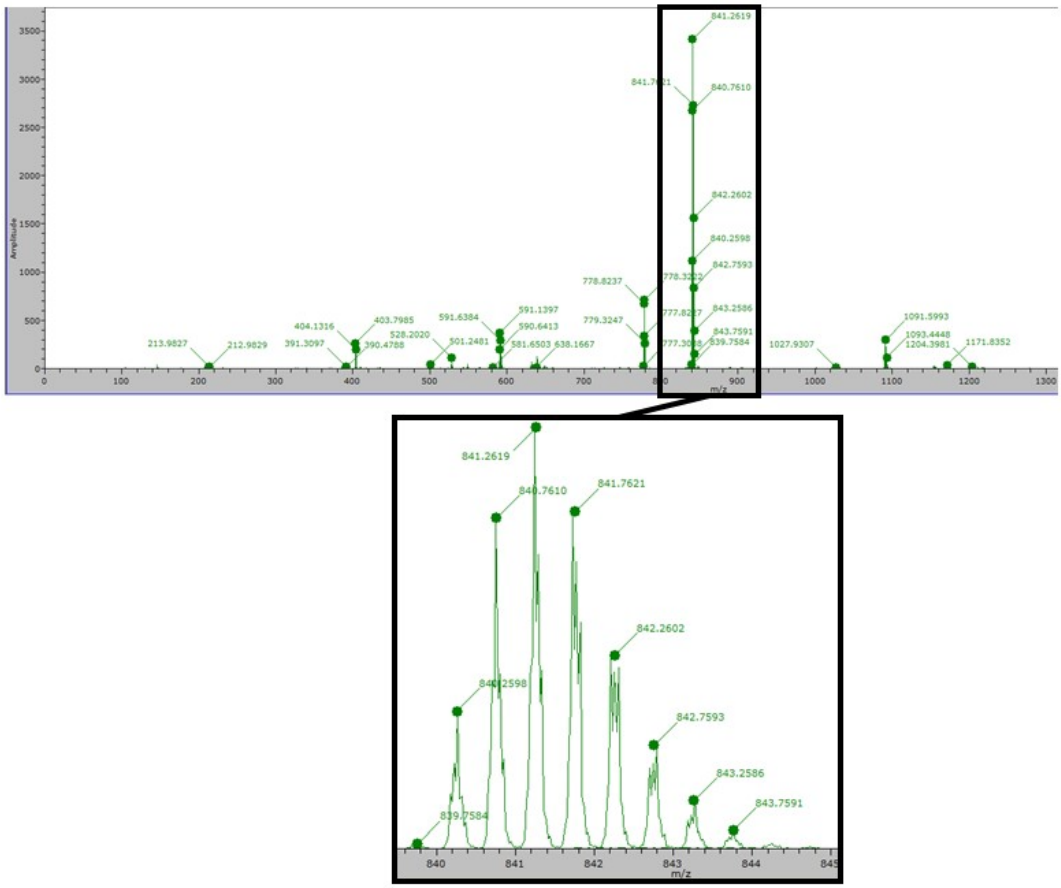

Figure S13. Mass spectrum of crystals of complex **6** dissolved in MeCN.

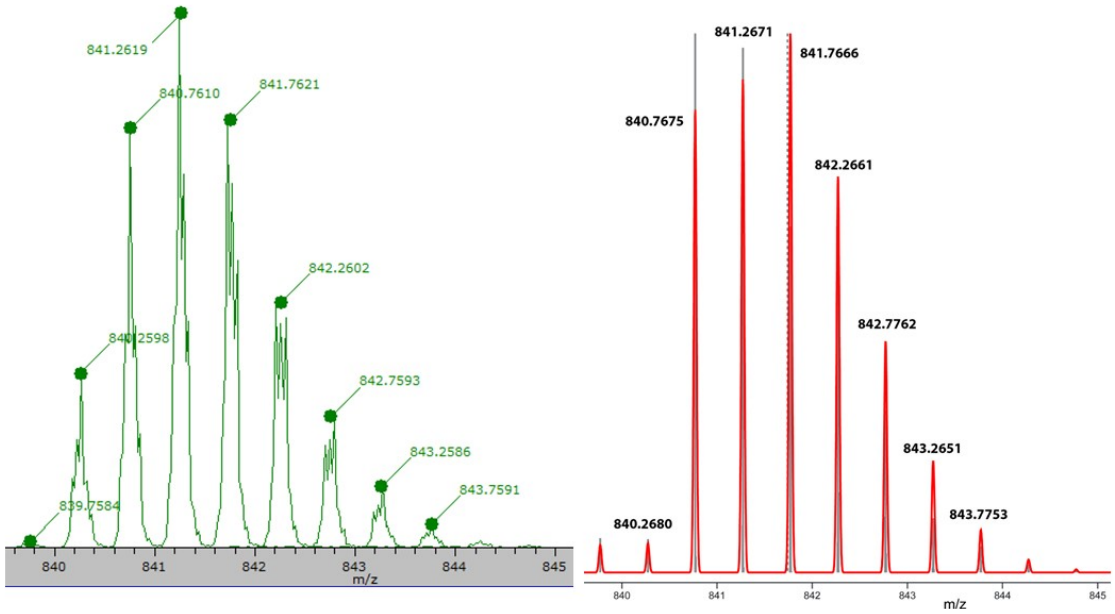

Figure S14. Comparison of the experimental (left) and simulated (right) mass spectrum of complex **6**. Simulation performed using Prot pi Mass Spectrum Simulator.[6]

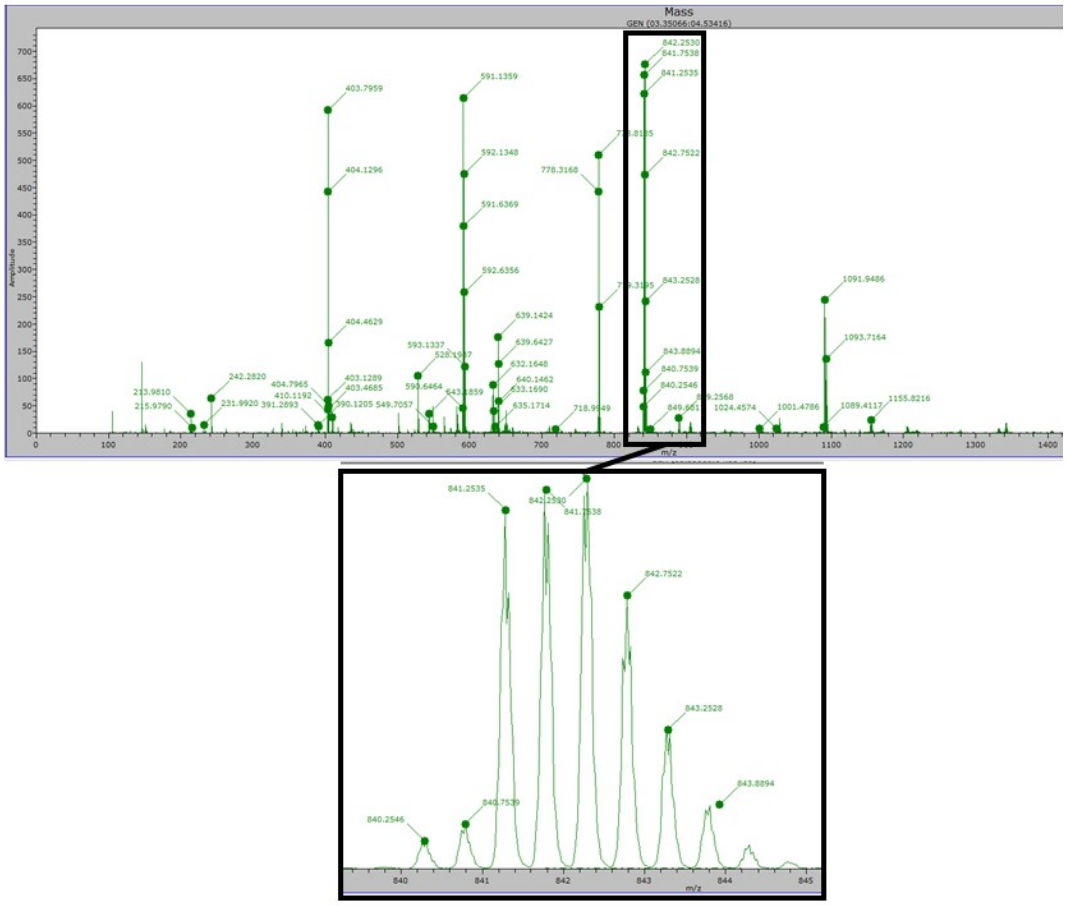

Figure S15. Mass spectrum of crystals of complex **7** dissolved in MeCN.

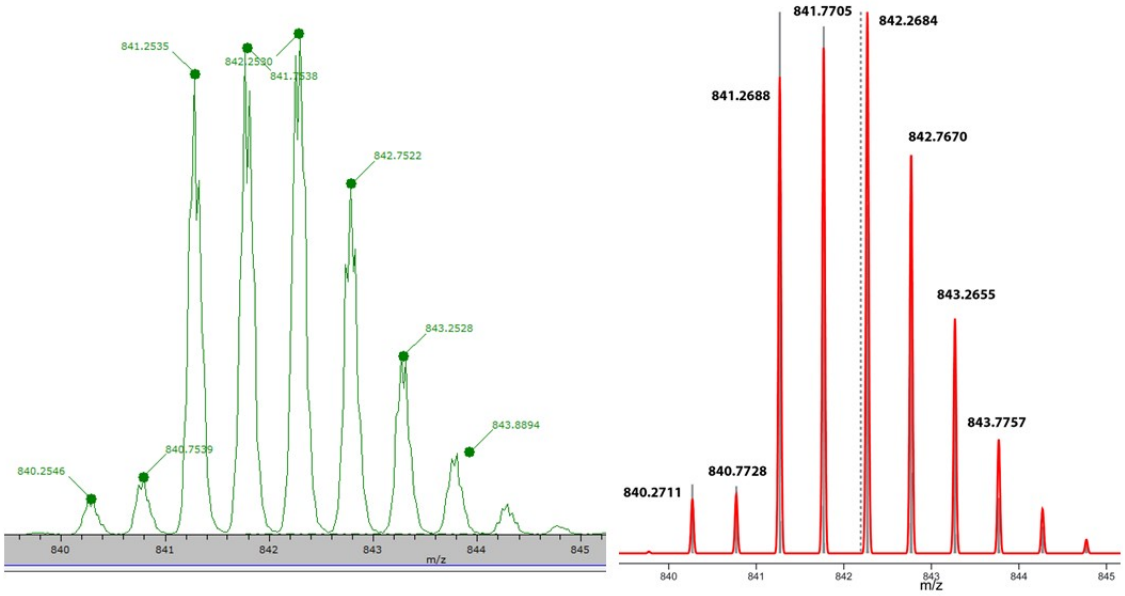

Figure S16. Comparison of the experimental (left) and simulated (right) mass spectrum of complex **7**. Simulation performed using Prot pi Mass Spectrum Simulator.[6]

6. X-ray crystallography

General Considerations: Crystalline samples were prepared in a glovebox by decanting residual supernatant and immersing the crystals under a protective layer of Paratone N oil. All samples were frozen in a container of dry ice prior to data collection. Data for **MTN**, **4**, **5**, and **7** were collected at the Advanced Light Source beamline 12.2.1 using a Bruker D85 three-circle diffractometer equipped with a PHOTON II CCD area detector using synchrotron radiation (λ = 0.7288 Å) from a Si(111) double crystal Si(111) monochromator. Data for **6** was collected at the UC Berkeley CheXRay crystallographic facility on a Rigaku Pilatus 200K diffractometer using Cu Kα radiation (λ = 1.542 Å). Structures were solved by intrinsic phasing using the SHELXT9 software package and refined using SHELXL10 in the OLEX2 interface.[7]

CCDC 2349134-2349138 contain the supplementary crystallographic data for this paper. These data can be obtained free of charge *via* www.ccdc.cam.ac.uk/dat_request/cif, or by emailing data_request@ccdc.cam.ac.uk, or by contacting the Cambridge Crystallographic Data Centre, 12 Union Road, Cambridge CB2 1EZ, UK; fax: +44 1223 336033

Structure Determination of MTN. The solid-state molecular structure of **MTN** exhibits two MTN molecules in the asymmetric unit. Half a molecule of diethyl ether was modeled in the asymmetric unit, along with one molecule of H_2O (of which, H-atoms were omitted). All non-hydrogen atoms were refined anisotropically and the H atoms were treated as riding models.

A residual electron density peak was noted near atom C63 of the diethyl ether molecule. This peak could not be assigned in a chemically reasonable fashion and was left as-is. There are no indications in the data to suggest twinning. Missing H-atoms are noted for atoms O2 and O3 of the two water molecules. H-atoms could not be reasonably located, assigned, or refined in the model as there is no clear H-bonding interactions. As such, these H-atoms were omitted from the model and left as-is.

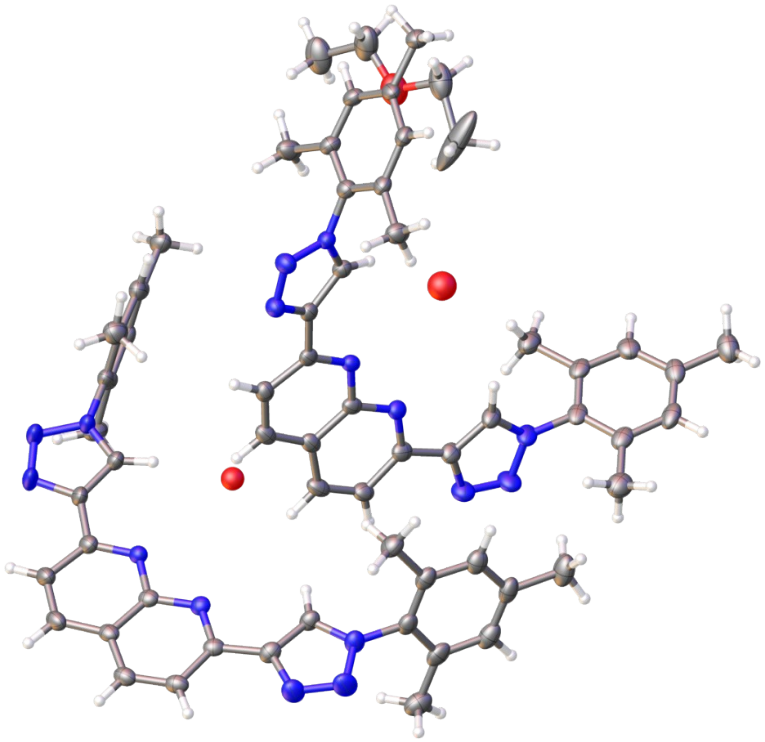

Figure S17. Solid-state molecular structure of **MTN**. Color scheme: C, gray; H, white; N, light blue; O, red.

Structure Determination of 4. The solid-state molecular structure of **4** exhibits disorder of all three triflimide anions in the asymmetric unit; the relative occupancies of these sites were refined with free variables. Various restraints and constraints (SADI, RIGU, SIMU, DFIX, DANG) were used to model the disordered triflimide molecules and to maintain physically reasonable anisotropic displacement parameters and geometries. Two molecules of THF were modeled in the asymmetric unit. All non-hydrogen atoms were refined anisotropically and the H atoms were treated as riding models.

A high Ueq as compared to its neighbors was noted on atom O7 of a disordered triflimide molecule. This is likely because it is a shared atom between two parts of disorder on the triflimide molecule. However, this oxygen atom could not be split across two positions in a reasonable fashion to improve the model and was left as-is.

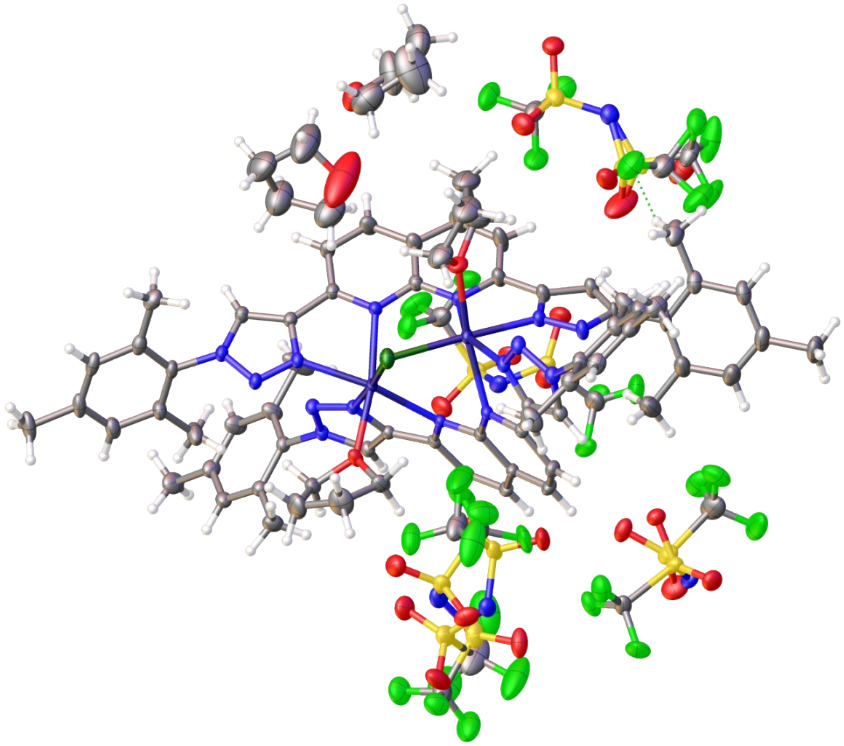

Figure S18. Solid-state molecular structure of **4**. Color scheme: C, gray; H, white; N, light blue; O, red; S, light yellow; F, light green; Cl, dark green; Fe, dark blue.

Structure Determination of 5. The solid-state molecular structure of **5** exhibits one molecule of **5** in the asymmetric unit. All non-hydrogen atoms were refined anisotropically and the H atoms were treated as riding models.

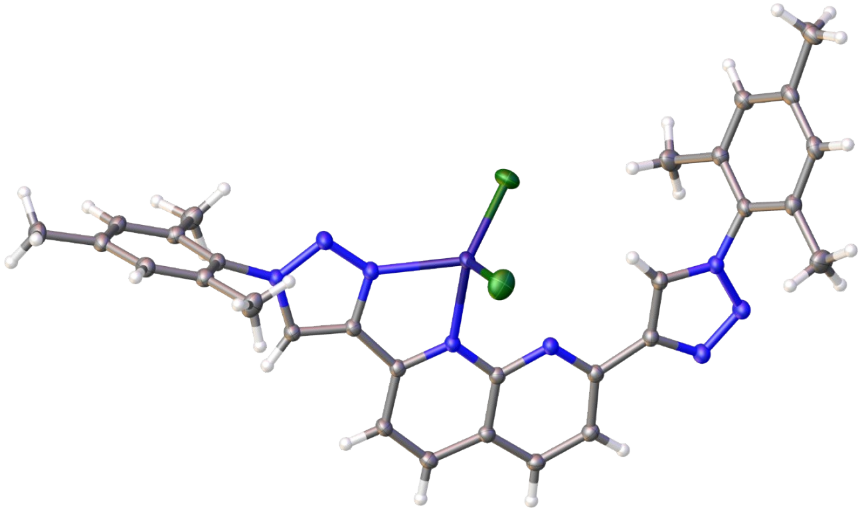

Figure S19. Solid-state molecular structure of **5**. Color scheme: C, gray; H, white; N, light blue; Cl, dark green; Fe, dark blue.

Structure Determination of 6. The solid-state molecular structure of **6** exhibits disorder of two mesityl groups in the asymmetric unit; the relative occupancies of these sites were refined with free variables. Various restraints and constraints (RIGU) were used to model the disordered molecular fragments and to maintain physically reasonable anisotropic displacement parameters and geometries. Two molecules of acetonitrile were modeled in the asymmetric unit. A solvent mask is applied that accounts for unresolved electron density. All non-hydrogen atoms were refined anisotropically and the H atoms were treated as riding models.

The metal sites in the structural model of **6** were refined as split sites occupied by Fe and Mn atoms in a fixed 0.5:0.5 ratio. An attempt was made to model each disordered Fe/Mn pair with free variables (so that the total site occupancy summed to one), with a SUMP constraint so that the total iron content per asymmetric unit is one. This resulted in occupancy values close to 0.5:0.5 at each disordered metal site; additionally, the refinement shift could not be converged owing to a fluctuation in one of the free variables for an iron atom. The metal site occupancies were therefore fixed to values of 0.5. As the metal-ligand bond distances at each metal site are within error, the metal atom identities cannot be readily distinguished by inspection of the metrical parameters; this is unsurprising in view of the fact that the ligand spheres are identical at each metal center, providing no site differentiation. Taken together, these observations point to the disordered model as the best description of the structure.

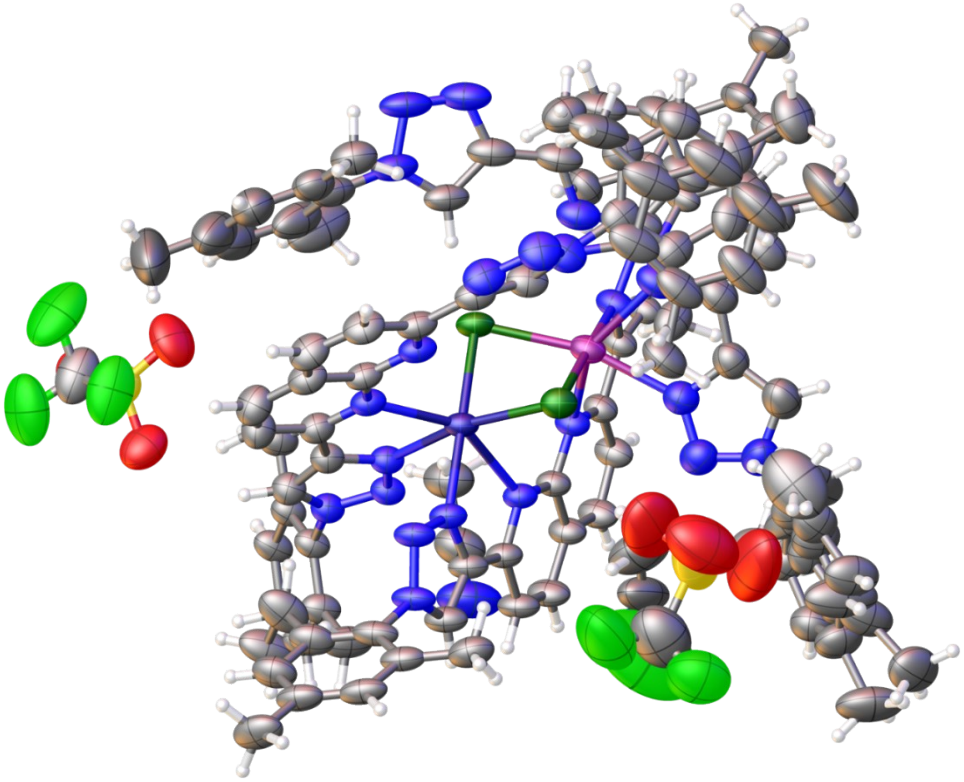

Figure S20. Solid-state molecular structure of **6.** Color scheme: C, gray; H, white; N, light blue; O, red; S, light yellow; F, light green; Cl, dark green; Fe, dark blue; Mn, purple.

Structure Determination of 7. The solid-state molecular structure of **7** exhibits disorder of two mesityl groups in the asymmetric unit; the relative occupancies of these sites were refined with free variables. Various restraints and constraints (RIGU) were used to model the disordered molecular fragments and to maintain physically reasonable anisotropic displacement parameters and geometries. Two molecules of acetonitrile were modeled in the asymmetric unit. A solvent mask is applied that accounts for unresolved electron density. All non-hydrogen atoms were refined anisotropically and the H atoms were treated as riding models.

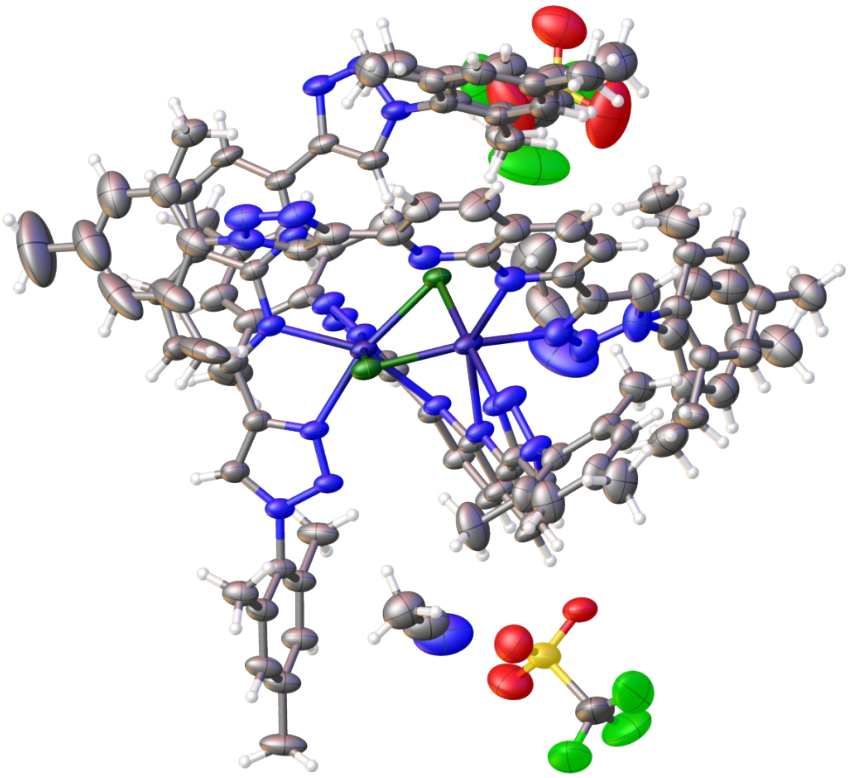

Figure S21. Solid-state molecular structure of **7.** Color scheme: C, gray; H, white; N, light blue; O, red; S, light yellow; F, light green; Cl, dark green; Fe, dark blue.

Compound	**MTN**	**4**	**5**
Empirical formula	$C_{62}H_{61}N_{16}O_{1.5}$	$C_{83}H_{88}ClF_{18}Fe_2N_{18}O_{16}S_6$	$C_{30}H_{28}Cl_2FeN_8$
Formula weight	1054.26	2275.22	627.35
Temperature/K	100.15	100.15	100.15
Crystal system	monoclinic	monoclinic	monoclinic
Space group	C2	$P2_1/n$	C2/c
a/Å	24.0364(12)	17.5489(5)	31.3189(13)
b/Å	14.7281(7)	15.0572(5)	12.0713(5)
c/Å	19.7560(16)	36.9438(11)	16.0669(7)
α/º	90	90	90
β/º	126.263(2)	94.9490(10)	107.5910(10)
γ/º	90	90	90
Volume/Å³	5639.2(6)	9725.5(5)	5780.2(4)
Z	4	4	8
Q_{calc}g/cm³	1.242	1.554	1.439
u/mm⁻¹	0.083	0.597	0.741
F(000)	2228.0	4668.0	2592.0
Crystal size/mm³	0.246 × 0.199 × 0.15	0.247 × 0.135 × 0.106	0.24 × 0.182 × 0.128
Radiation	synchrotron (λ = 0.7288)	synchrotron (λ = 0.7288)	MoKa (λ = 0.71073)
2Θ range for data collection/°	3.476 to 52.21	3.77 to 58.286	4.258 to 61.11
Index ranges	-28 ≤ h ≤ 28, -17 ≤ k ≤ 17, -23 ≤ l ≤ 23	-23 ≤ h ≤ 23, -20 ≤ k ≤ 20, -49 ≤ l ≤ 49	-44 ≤ h ≤ 44, -17 ≤ k ≤ 16, -22 ≤ l ≤ 22
Reflections collected	37796	158667	51057
Independent reflections	10328 [R_{int} = 0.0698, R_{sigma} = 0.0602]	24252 [R_{int} = 0.0591, R_{sigma} = 0.0389]	8850 [R_{int} = 0.0423, R_{sigma} = 0.0288]
Data/restraints/ parameters	10328/55/748	24252/778/1626	8850/0/376
Goodness-of-fit on F²	1.059	1.040	1.040
Final R indexes [[>=2σ (I)]	R_1 = 0.0598, wR_2 = 0.1584	R_1 = 0.0515, wR_2 = 0.1417	R_1 = 0.0327, wR_2 = 0.0887
Final R indexes [all data]	R_1 = 0.0630, wR_2 = 0.1616	R_1 = 0.0690, wR_2 = 0.1536	R_1 = 0.0351, wR_2 = 0.0903
Largest diff. peak/hole / e Å⁻³	1.03/-0.44	1.29/-0.85	0.52/-0.41
Flack Parameter	-0.1(6)	-	-

Compound	**6**	**7**
Empirical formula	$C_{102}H_{99}Cl_2F_6FeMnN_{29}O_6S_2$	$C_{96}H_{90}Cl_2F_6Fe_2N_{26}O_6S_2$
Formula weight	2186.91	2064.65
Temperature/K	100.15	100.15
Crystal system	triclinic	triclinic
Space group	P-1	P-1
a/Å	14.1048(2)	14.0576(10)
b/Å	19.0576(3)	19.1460(14)
c/Å	22.1206(3)	22.1777(16)
α/º	78.5920(10)	78.520(3)
β/º	75.1680(10)	74.856(3)
γ/º	71.179(2)	72.035(3)
Volume/Å^3	5397.34(15)	5435.1(7)
Z	2	2
Q_{calc}g/cm^3	1.346	1.262
u/mm^{-1}	3.486	0.452
F(000)	Cu Kα (λ = 1.54184)	2136.0
Crystal size/mm^3	0.246 × 0.167 × 0.159	0.028 × 0.008 × 0.008
Radiation	Cu Kα (λ = 1.54184)	synchrotron (λ = 0.7288)
2Θ range for data collection/°	6.048 to 149.006	2.836 to 53.866
Index ranges	-17 ≤ h ≤ 17, -23 ≤ k ≤ 23, -25 ≤ l ≤ 27	-17 ≤ h ≤ 17, -23 ≤ k ≤ 23, -27 ≤ l ≤ 27
Reflections collected	230269	77076
Independent reflections	22029 [R_{int} = 0.0788, R_{sigma} = 0.0311]	21664 [R_{int} = 0.0428, R_{sigma} = 0.0413]
Data/restraints/ parameters	22029/63/1403	21664/252/1427
Goodness-of-fit on F^2	1.068	1.057
Final R indexes [[>=2σ (I)]	R_1 = 0.0692, wR_2 = 0.1974	R_1 = 0.0603, wR_2 = 0.1831
Final R indexes [all data]	R_1 = 0.0826, wR_2 = 0.2099	R_1 = 0.0715, wR_2 = 0.1925
Largest diff. peak/hole / e Å^{-3}	0.46/-0.89	1.24/-0.75
Flack Parameter	-	-

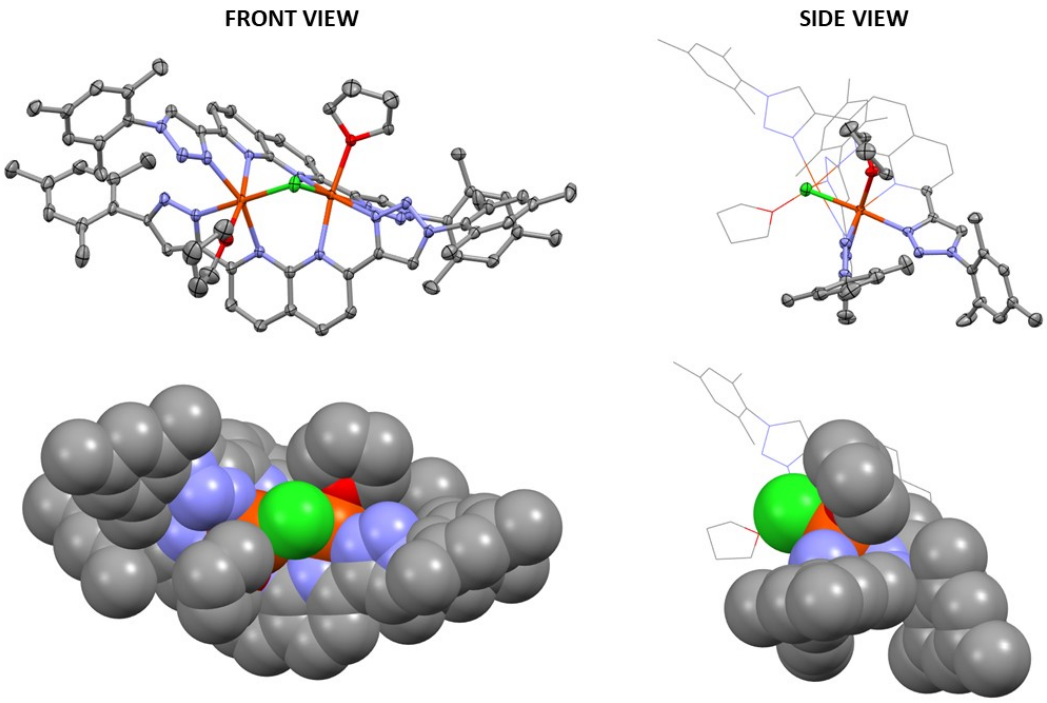

Figure S22. Spacefill representation of the solid-state structure of complex **4**.

7. DFT calculations

Computational Details

DFT calculations were performed at the Molecular Graphics and Computation Facility of the University of California, Berkeley, using the Gaussian 16 suite of programs.[8] A relaxed potential energy surface scan calculation on one of the side-arms of the **MTN** ligand using the PBE0 functional,[9] as implemented in the G16 software along with Grimme's D3 dispersion correction. [10] The H, C and N atoms were described with the 6-31g(d,p) basis set.[11]

Potential Energy Surface Scan

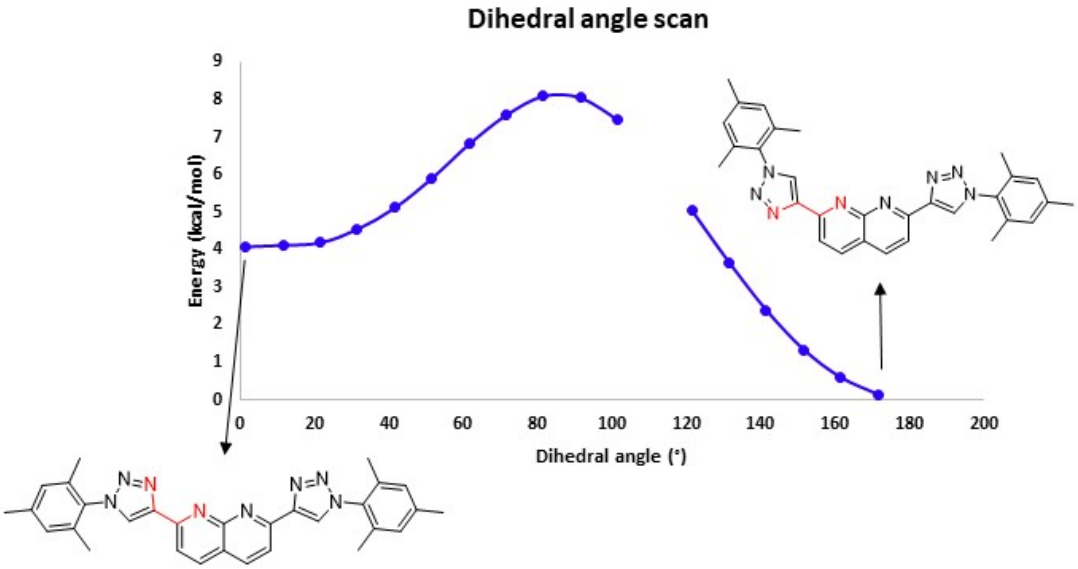

Figure S23. Potential energy surface scan of the dihedral angle highlighted in red of the **MTN** ligand. The absence of data at 111° is due to the fact that convergence criteria were not met during the PES calculation.

8. EPR Spectroscopy

The X-band EPR spectrum was simulated using a single spin system of S = 5/2, g = 2.00, A 55Mn= 250 MHz, D ~ 1900 MHz (0.063 cm-1) and E/D of 0.25. Following a previous method,[12] a gaussian distribution of D was considered to account for the overall spectral lineshape (see Fig. S25-S26 for simulations with different D and E/D). The magnitude of both D and E/D are similar to other Mn2+ systems with N3O3 ligand environment.[13]

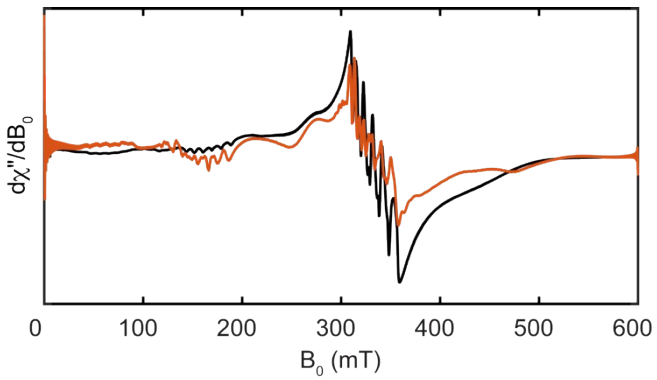

Figure S24. X-band EPR spectrum of **6** (10K, 0.2 mW) with simulation shown in red. Simulation parameters: *S* = 5/2, *g* = 1.98, *A* ^{55}Mn = 250 MHz, *D* = 1900 MHz, *E*/*D* = 0.25.

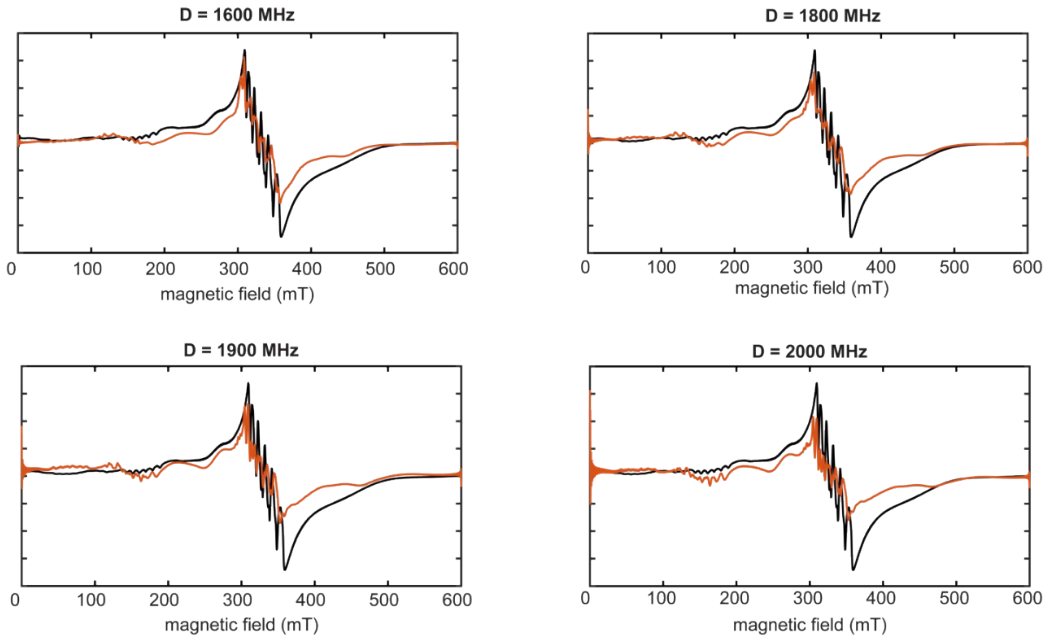

Fig S25. Simulations (in red) of the X-band spectrum with varying *D* values with fixed *E*/*D* = 0.25.

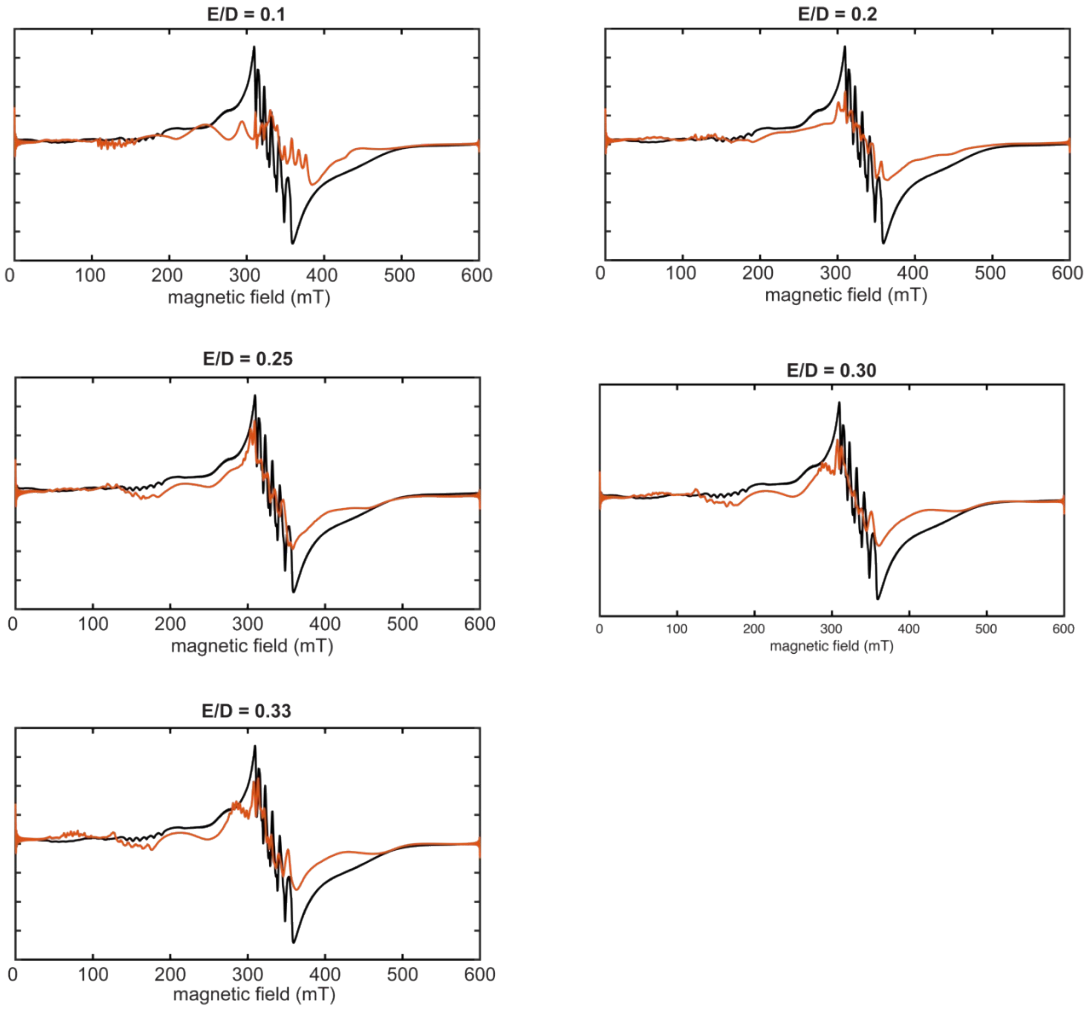

Fig S26. Simulations (in red) of the X-band spectrum with varying *E*/*D*.

9. DC magnetization measurements

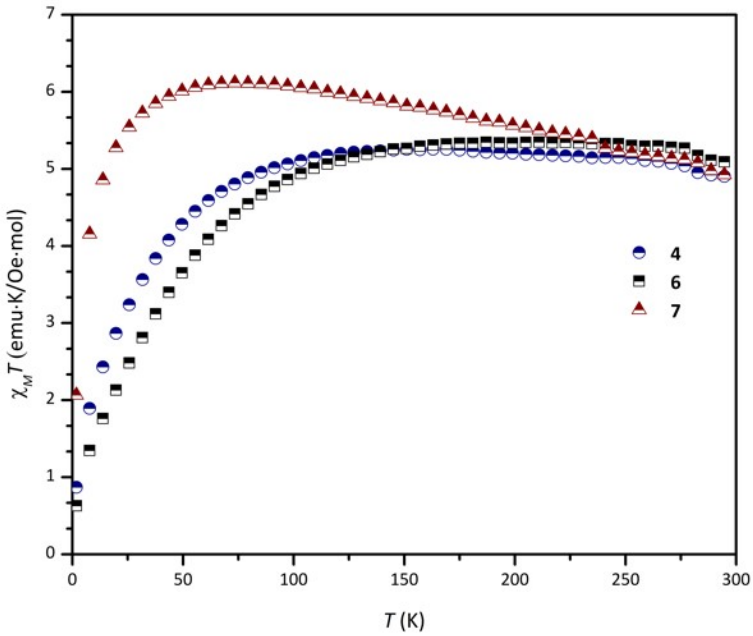

Figure S27. Temperature dependence of the molar magnetic susceptibility plotted as $\chi_M T$ of **4** (blue circles), **6** (black squares), and **7** (red triangles) at 1 T from 1.8 K to 300 K.

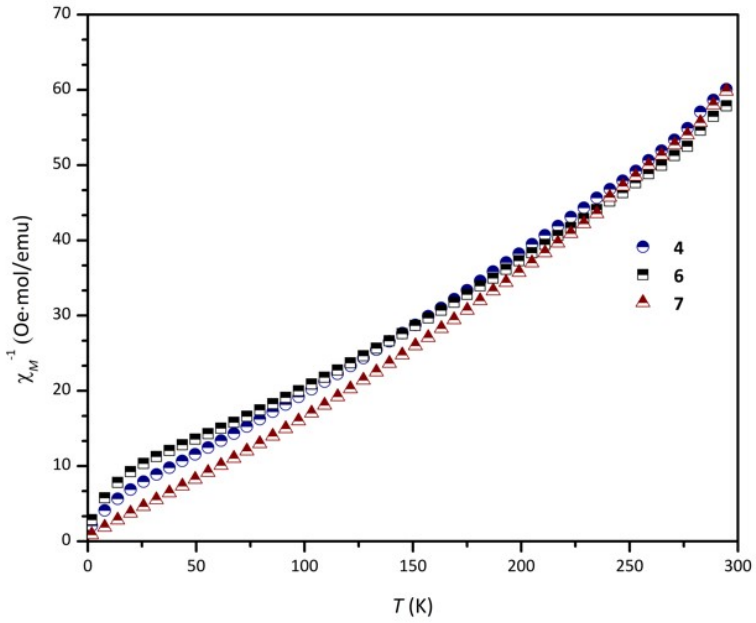

Figure S28. Inverse molar magnetic susceptibility of **4** (blue circle), **6** (black square), and **7** (red triangles) at 1 T from 1.8 K to 300 K. Curie-Weiss fits were taken at high T (linear regime) to obtain the Curie constant (C), Curie-Weiss temperature (θ_{CW}), and μ_{eff}. (The T range used for **4**, **6**, and **7** were 26.7-276.7, 25.7-295.6, and 13.7-298.6 K, respectively.)

10. References

1) G. R. Newkome, S. J. Garbis, V. K. Majestic, F. R. Fronczek and G. Chiari, *J. Org. Chem.* **1981**, *46*, 833-839.

2) a) R. Ziessel, J. Suffert and M-T. Youinou, *J. Org. Chem.,* **1996**, *61*, 6535-6546. b) J. Y. Hwang, H-G. Jeon, Y. R. Choi, J. Kim, P. Kang, S. Lee and K-S. Jeong, *Org. Lett.* **2017**, *19*, 5625-5628.

3) D. G. Brown, N. Sanguantrakun, B. Schulze, U. S. Schubert and C. P. Berlinguette, *J. Am. Chem. Soc.,* **2012**, *134*, 12354-12357.

4) D. A. Roberts, B. S. Pilgrim, J. D. Cooper, T. K. Ronson, S. Zarra and J. R. Nitschke, *J. Am. Chem. Soc.,* **2015**, *137*, 10068-10071.

5) S. Stoll, A. Schweiger. *J. Magn. Reson.* **2006**, *178*, 42-55.

6) https://www.protpi.ch/Calculator/MassSpecSimulator

7) O. V. Dolomanov, L. J. Bourhis, R. J. Gildea, J. A. K. Howard, H. Puschmann. *J. Appl. Cryst.* **2009**, *42*, 339–341.

8) Gaussian 16, Revision C.01, M. J. Frisch, G. W. Trucks, H. B. Schlegel, G. E. Scuseria, M. A. Robb, J. R. Cheeseman, G. Scalmani, V. Barone, G. A. Petersson, H. Nakatsuji, X. Li, M. Caricato, A. V. Marenich, J. Bloino, B. G. Janesko, R. Gomperts, B. Mennucci, H. P. Hratchian, J. V. Ortiz, A. F. Izmaylov, J. L. Sonnenberg, D. Williams-Young, F. Ding, F. Lipparini, F. Egidi, J. Goings, B. Peng, A. Petrone, T. Henderson, D. Ranasinghe, V. G. Zakrzewski, J. Gao, N. Rega, G. Zheng, W. Liang, M. Hada, M. Ehara, K. Toyota, R. Fukuda, J. Hasegawa, M. Ishida, T. Nakajima, Y. Honda, O. Kitao, H. Nakai, T. Vreven, K. Throssell, J. A. Montgomery, Jr., J. E. Peralta, F. Ogliaro, M. J. Bearpark, J. J. Heyd, E. N. Brothers, K. N. Kudin, V. N. Staroverov, T. A. Keith, R. Kobayashi, J. Normand, K. Raghavachari, A. P. Rendell, J. C. Burant, S. S. Iyengar, J. Tomasi, M. Cossi, J. M. Millam, M. Klene, C. Adamo, R. Cammi, J. W. Ochterski, R. L. Martin, K. Morokuma, O. Farkas, J. B. Foresman, and D. J. Fox, Gaussian, Inc., Wallingford CT, 2016.

9) C. Adamo, V. Barone. *J. Chem. Phys.* **1999**, *110*, 6158-6170.

10) S. Grimme, J. Anthony, S. Ehrlich, H. Krieg. *J. Chem. Phys.* **2010**, *132*, 154104-154119.

11) a) W. J. Hehre, R. Ditchfield, J. A. Pople, *J. Chem. Phys.* **1972**, *56*, 2257-2261; b) P.C. Hariharan, J. A. Pople, *Theor. Chim. Acta.,* **1973**, *28*, 213-222

12) D. M. Gagnon, M. B. Brophy, S. E. J. Bowman, T. A. Stich, C. L. Drennan, R. D. Britt, E. M. Nolan, *J. Am. Chem. Soc.,* **2015**, *137*, 3004-3016.

13) T. A. Stich, S. Lahiri, G. Yeagle, M. Dicus, M. Brynda, A. Gunn, C. Aznar, V. J. DeRose, R. D. Britt, *Appl. Magn. Reson.* **2007**, *31*, 321-341.